

# Group analysis, DNS and modeling of a turbulent channel flow with streamwise rotation

By M. Oberlack<sup>1</sup>, W. Cabot, AND M. M. Rogers

The turbulent channel flow with streamwise rotation has been investigated by means of several different analytical, numerical, and modeling approaches. Lie group analysis of the two-point correlation equations led to linear scaling laws for the streamwise mean velocity. In addition it was found that a cross flow in spanwise direction is induced, which may also exhibit a linear region. By further analysis of the two-point correlation equation, it is shown that all six components of the Reynolds stress tensor are non-zero. In addition certain symmetries and skew-symmetries about the centerline have been established for all flow quantities. All the latter findings of the analysis have been very well verified by means of direct numerical calculations. The flow has also been tackled by LES and second-moment closure models. The dynamic LES captured most of the theoretical and DNS findings quantitatively. The second-moment closure model was able to capture most of the basic trends, but any quantitative agreement could not be achieved.

---

## 1. Introduction

During the development of the symmetry theory in Oberlack (1997a), it was noticed that there may be one additional turbulent scaling law which was not mentioned since no experimental or DNS data were available. This is the turbulent channel flow rotating about the streamwise direction. A sketch of the flow geometry is given in Fig. 1.

The flow appears to have several common features with the classical rotating channel flow (Johnston *et al.* 1972) but also has some very distinct characteristics. The classical case considers the rotation of a turbulent channel flow about the spanwise direction ( $x_3$ ). In this flow the mean stream lines follow plane spirals. In contrast to this, mean stream lines of the present flow exhibit corkscrew-like spirals. However, the most obvious difference between the two cases may be the induction of a mean velocity in  $x_3$ -direction. This cross flow can be deduced by investigating the mean momentum equation and the Reynolds stress transport equation.

It is interesting to note that the induced cross flow is a property of the turbulent flow and may not be deduced from the equations for laminar flows.

Similar to the classical case, it will be shown that the only self-similar mean velocity profiles are linear functions

$$\bar{u}_1 = A_1\Omega_1x_2 + B_1 \quad \text{and} \quad \bar{u}_3 = A_2\Omega_1x_2 + B_2$$

<sup>1</sup> Inst. für Technische Mechanik, RWTH-Aachen, Germany

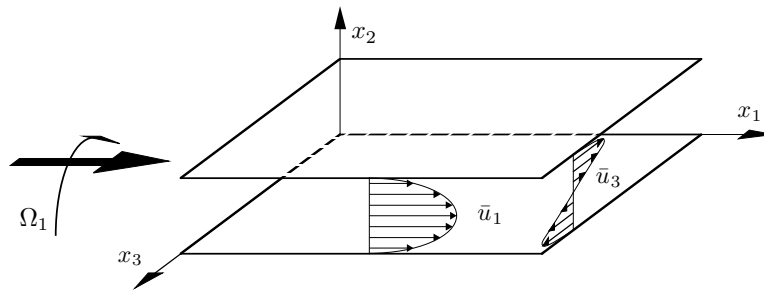


FIGURE 1. Sketch of the flow geometry of a turbulent channel flow with streamwise rotating.

to be derived in the subsequent sections. In both the present and the classical case, the mean velocities scale on the rotation rate.

Nevertheless, it is anticipated that the general appearance of the mean velocity profile in  $x_1$ -direction is very different from the classical case. Since the reflection symmetry about the center line is not broken, the mean velocity may stay symmetrical. In Oberlack (1997a) it was observed that, except for the log-law, the highest degree of symmetry is usually obtained in flow regions with the weakest wall influence. Hence, it is expected that two linear regions may emerge near the center region. To the best knowledge of the authors, it appears that the above mentioned test case has never been described in the literature.

The paper is organized as follows. In the next section three different analyses are presented. The one which actually initiated the project is Lie group analysis of the present flow, which suggested the linear velocity profiles. Besides the latter analysis, global time scales of the flow will be investigated which indicate the location of the linear regions. In the final analysis, it will be examined which flow quantity is symmetric or antisymmetric about the centerline of the channel. In the section thereafter, a DNS of the rotating channel flow is presented. Mean velocities and statistical quantities for different rotation rates will be established. Finally, the present test case is to be tackled with turbulence models. Results from second-moment closure models and LES are shown.

## 2. Analysis

The basis for the analysis of the present flow geometry in Subsections 2.2 and 2.3 is the mean momentum equation and the two-point velocity correlation equation in a rotating frame of reference, which are given respectively by

$$0 = -\frac{1}{\rho} \frac{\partial \bar{p}}{\partial x_1} - \frac{\partial \overline{u_1 u_2}}{\partial x_2} + \nu \frac{\partial^2 \bar{u}_1}{\partial x_2^2} \quad (1a)$$

$$0 = -\frac{1}{\rho} \frac{\partial \bar{p}}{\partial x_2} - \frac{\partial \overline{u_2 u_2}}{\partial x_2} - 2\Omega_1 \bar{u}_3 \quad (1b)$$

$$0 = -\frac{\partial \overline{u_2 u_3}}{\partial x_2} + \nu \frac{\partial^2 \bar{u}_3}{\partial x_2^2} \quad (1c)$$

and

$$\begin{aligned}
 0 = & -R_{2j}\delta_{i1}\frac{d\bar{u}_1(x_2)}{dx_2} - R_{2j}\delta_{i3}\frac{d\bar{u}_3(x_2)}{dx_2} - R_{i2}\delta_{j1}\frac{d\bar{u}_1(x_2+r_2)}{d(x_2+r_2)} - R_{i2}\delta_{j3}\frac{d\bar{u}_3(x_2+r_2)}{d(x_2+r_2)} \\
 & - [\bar{u}_1(x_2+r_2) - \bar{u}_1(x_2)]\frac{\partial R_{ij}}{\partial r_1} - [\bar{u}_3(x_2+r_2) - \bar{u}_3(x_2)]\frac{\partial R_{ij}}{\partial r_3} \\
 & - \frac{1}{\rho}\left[\delta_{i2}\frac{\partial \overline{pu_j}}{\partial x_2} - \frac{\partial \overline{pu_j}}{\partial r_i} + \frac{\partial \overline{u_i p}}{\partial r_j}\right] + \nu\left[\frac{\partial^2 R_{ij}}{\partial x_2 \partial x_2} - 2\frac{\partial^2 R_{ij}}{\partial x_2 \partial r_2} + 2\frac{\partial^2 R_{ij}}{\partial r_k \partial r_k}\right] \\
 & - \frac{\partial R_{(i2)j}}{\partial x_2} + \frac{\partial}{\partial r_k}\left[R_{(ik)j} - R_{i(jk)}\right] - 2\Omega_1[e_{1li}R_{lj} + e_{1lj}R_{il}] \quad (2)
 \end{aligned}$$

(see, e.g., Rotta 1972 and Hinze 1959);  $\bar{u}_i$ ,  $\bar{p}$ ,  $\overline{u_i u_j}$ ,  $\nu$ ,  $\Omega_1$ , and  $e_{ijk}$  are the respectively the mean velocity, the mean pressure, the Reynolds stress tensor, the dynamic viscosity, the rotation rate in  $x_1$ -direction, and the alternation tensor. The five two-point correlation tensor functions which appear in Eq. (2) are defined as

$$R_{ij}(\mathbf{x}, \mathbf{r}; t) = \overline{u_i(\mathbf{x}, t) u_j(\mathbf{x}^{(1)}, t)} , \quad (3a)$$

$$\overline{pu_j}(\mathbf{x}, \mathbf{r}; t) = \overline{p(\mathbf{x}, t) u_j(\mathbf{x}^{(1)}, t)} , \quad \overline{u_j p}(\mathbf{x}, \mathbf{r}; t) = \overline{u_j(\mathbf{x}, t) p(\mathbf{x}^{(1)}, t)} , \quad (3b)$$

$$\begin{aligned}
 R_{(ik)j}(\mathbf{x}, \mathbf{r}; t) &= \overline{u_i(\mathbf{x}, t) u_k(\mathbf{x}, t) u_j(\mathbf{x}^{(1)}, t)} , \\
 R_{i(jk)}(\mathbf{x}, \mathbf{r}; t) &= \overline{u_i(\mathbf{x}, t) u_j(\mathbf{x}^{(1)}, t) u_k(\mathbf{x}^{(1)}, t)} , \quad (3c)
 \end{aligned}$$

where  $u_i$  and  $p$  correspond to the fluctuating quantities. The tensors (3a-c) are functions of the physical and the correlation space coordinates  $\mathbf{x}$  and  $\mathbf{r} = \mathbf{x}^{(1)} - \mathbf{x}$  respectively. For the present case all statistical quantities only depend on the wall-normal coordinate  $x_2$  and the correlation coordinate  $\mathbf{r}$ . The double two-point correlation tensor  $R_{ij}$ , later on simply referred to as two-point correlation, converges to the Reynolds stress tensor  $\overline{u_i u_j}$  in the limit of zero separation  $|\mathbf{r}|$ :

$$\overline{u_i u_j}(\mathbf{x}) = \lim_{r \rightarrow 0} R_{ij}(\mathbf{x}, \mathbf{r}) . \quad (4)$$

It should be noted that the two-point correlation equation only contains the triple correlations as unknown terms. For both two-point velocity-pressure correlations,  $\overline{u_i p}$  and  $\overline{pu_j}$  a Poisson equation may be derived (see, e.g., Oberlack 1994, 1995). In addition, all dependent variables in (2) must satisfy the continuity conditions

$$\frac{\partial R_{ij}}{\partial x_i} - \frac{\partial R_{ij}}{\partial r_i} = 0 , \quad \frac{\partial R_{ij}}{\partial r_j} = 0 , \quad \frac{\partial \overline{pu_j}}{\partial r_j} = 0 \quad \text{and} \quad \frac{\partial \overline{u_i p}}{\partial x_i} - \frac{\partial \overline{u_i p}}{\partial r_i} = 0 . \quad (5)$$

For the understanding of the self-similarity of the two-point correlation equation given further below, two identities may give some interesting insight in the structure

of the two-point correlation function. They can easily be derived from a geometrical consideration by interchanging the two points  $\mathbf{x}$  and  $\mathbf{x}^{(1)} = \mathbf{x} + \mathbf{r}$ :

$$R_{ij}(\mathbf{x}, \mathbf{r}) = R_{ji}(\mathbf{x} + \mathbf{r}, -\mathbf{r}) \quad , \quad \overline{u_i p}(\mathbf{x}, \mathbf{r}) = \overline{p u_i}(\mathbf{x} + \mathbf{r}, -\mathbf{r}) \quad . \quad (6)$$

The former is particularly interesting for the trace elements of  $R_{ij}$  since it defines a functional equation in real- and correlation-space. There exists a similar identity to (6) for the triple correlation, which will not be utilized here.

Some fundamental properties of the flow can already be read from Eq. (1a-c). For high Reynolds number flows, viscous transport terms are only significant in the near-wall region. In regions sufficiently apart from solid walls, the viscous terms may be neglected to leading order, and the balance is dominated by the pressure and the turbulent stresses.

From Eq. (1a) the usual linear turbulent shear stress profile for  $\overline{u_1 u_2}$  may be derived because the pressure-gradient in the streamwise ( $x_1$ ) direction is constant. Since no pressure-gradient in the spanwise ( $x_3$ ) direction is present, it can be deduced from Eq. (1c) that the shear stress  $\overline{u_2 u_3}$  is uniform. Equation (1b) only determines the pressure-gradient in wall-normal direction. Though it is the only mean momentum equation containing the Coriolis force, it has no influence on the mean velocity. It will be seen later that the mean velocity is only determined by the turbulent stresses. This is similar to the usual non-rotating channel flow in which no information for the mean flow can be determined from the mean momentum equation.

At this point it will be anticipated that besides the shear stress  $\overline{u_2 u_3}$  the additional shear stress  $\overline{u_1 u_3}$  is induced due the rotation. This can be taken from Eq. (2) in which a Coriolis term appears in the  $R_{13}$ -equation. From the structure of the “13” equation, it appears that the Coriolis term may not be solely balanced by the pressure-velocity correlation and by the triple correlation. One may naturally expect that the term  $[\overline{u_k}(x_2 + r_2) - \overline{u_k}(x_2)] \partial R_{13} / \partial r_k$  may also contribute to the balance in the equation. Hence  $\overline{u_1 u_3}$  may be non-zero though this stress has no counterpart in the mean velocities in an eddy-viscosity sense.

### 2.1 Time-scale analysis

In the present subsection the characteristic time scales of the viscous sublayer and the universal logarithmic region will be compared with the characteristic time scale of the rotation rate. The latter is defined as

$$t_\Omega \equiv \frac{1}{\Omega} \quad (7)$$

where  $\Omega$  is the rotation rate about the  $x_1$ -direction, also denoted by  $\Omega_1$ .

The characteristic time scale of the viscous sublayer and the universal logarithmic region are

$$t_\nu \equiv \frac{\nu}{u_\tau^2} \quad \text{and} \quad t_{\log} \equiv \frac{y}{u_\tau} \quad (8)$$

respectively where  $u_\tau$  is the “friction velocity” defined as  $u_\tau = \sqrt{\nu \left. \frac{\partial \bar{u}_1}{\partial x_2} \right|_{\text{wall}}}$ . For sufficiently high Reynolds number,  $t_\nu$  is a fixed small quantity while  $t_{\log}$  increases with the distance from the wall. Comparing the ratio of the latter flow time scales with the rotation time scale we respectively obtain

$$T_1 = \frac{t_\nu}{t_\Omega} = \frac{\nu\Omega}{u_\tau^2} = \frac{\text{Ro}}{2\text{Re}} \quad (9)$$

and

$$T_2 = \frac{t_{\log}}{t_\Omega} = \frac{y\Omega}{u_\tau} = \text{Ro} \frac{y}{h} , \quad (10)$$

where  $\text{Re}_\tau = hu_\tau/2\nu$  and  $\text{Ro} = \Omega h/u_\tau$ .

For zero rotation rate both quantities are exactly zero. However, assuming  $\text{Ro}$  of the order  $\mathcal{O}(1)$  and supposing  $\text{Re}$  to be a large parameter, the time scale ratio  $T_1$  is a small quantity. Hence it is concluded that the rotation only perturbs the viscous sublayer, and a significant change may not be observed.

Considering the same order of magnitude assumptions for  $\text{Ro}$  as above, it can be concluded that  $T_2$  may only be a small parameter for small  $y/h$ . This is the flow region close to the wall and next to the viscous sublayer. In contrast, if  $y/h$  is of order  $\mathcal{O}(1)$ ,  $T_2$  may become an order  $\mathcal{O}(1)$  parameter. Consequently, we conclude that this is the flow region which is affected most by the system rotation. In this region system rotation is a leading order effect. In addition we conclude that the region which is affected most by the rotation extends further to the wall with increasing rotation rate. The mean velocity of a turbulent channel flow is only weakly affected by the system rotation in the near-wall region. However, system rotation has a substantial effect on regions sufficiently far from the wall such as the logarithmic region up to the centerline.

In fact this global effect has been observed both in experiments and in DNS for the classical rotating channel flow with  $x_3$  as the rotation axis (see e.g. Johnston *et al.* 1972, Kristoffersen & Andersson 1993). In contrast to the present case the classical rotating channel case does not reveal a symmetric mean velocity profile about the centerline. Instead a skewed mean velocity profile in the center part of the channel is observed.

## 2.2 Reflection symmetry of statistical flow quantities about the centerline

Reflection symmetries can be obtained by finding transformations of the form  $\tilde{\phi} = -\phi$  where  $\phi$  may represent any dependent and independent variable. The following is observed in a variety of different channel type of flows such as the usual turbulent Poiseuille and the turbulent Couette flow. If the corresponding equations and boundary conditions admit a certain reflection symmetry about the centerline, this is also verified for all statistical quantities.

For the present problem the system (2) and (5) admits the reflection symmetry where the variables are respectively separated as independent variables, mean quantities, and statistical quantities

$$\tilde{x}_1 = x_1 , \quad \tilde{x}_2 = -x_2 , \quad \tilde{x}_3 = -x_3 , \quad \tilde{r}_1 = r_1 , \quad \tilde{r}_2 = -r_2 , \quad \tilde{r}_3 = -r_3 , \quad (11a)$$

$$\tilde{u}_1 = \bar{u}_1 \quad , \quad \tilde{u}_3 = -\bar{u}_3 \quad , \quad \tilde{p} = \bar{p} \quad , \quad (11b)$$

$$\begin{pmatrix} \tilde{R}_{11} & \tilde{R}_{12} & \tilde{R}_{13} \\ \tilde{R}_{21} & \tilde{R}_{22} & \tilde{R}_{23} \\ \tilde{R}_{31} & \tilde{R}_{32} & \tilde{R}_{33} \end{pmatrix} = \begin{pmatrix} R_{11} & -R_{12} & -R_{13} \\ -R_{21} & R_{22} & R_{23} \\ -R_{31} & R_{32} & R_{33} \end{pmatrix} \quad , \quad (11c)$$

$$\begin{pmatrix} \overline{\tilde{p}u_1} \\ \overline{\tilde{p}u_2} \\ \overline{\tilde{p}u_3} \end{pmatrix} = \begin{pmatrix} \overline{pu_1} \\ -\overline{pu_2} \\ -\overline{pu_3} \end{pmatrix} \quad \text{and} \quad \begin{pmatrix} \overline{\tilde{u}_1\tilde{p}} \\ \overline{\tilde{u}_2\tilde{p}} \\ \overline{\tilde{u}_3\tilde{p}} \end{pmatrix} = \begin{pmatrix} \overline{u_1\bar{p}} \\ -\overline{u_2\bar{p}} \\ -\overline{u_3\bar{p}} \end{pmatrix} \quad . \quad (11d)$$

The latter reflection symmetries can be generalized as such that any other statistical one-, two-, and multi-point quantity can be determined from the fluctuation quantities according to the transformation for the fluctuations

$$\tilde{u}_1 = u_1 \quad , \quad \tilde{u}_2 = -u_2 \quad , \quad \tilde{u}_3 = -u_3 \quad , \quad \tilde{p} = p \quad . \quad (12)$$

For example, the transformation of the two-point triple correlations  $R_{(ik)j}$  and  $R_{i(jk)}$  which are not stated above can be determined in a similar manner.

From (11b) it can be determined that  $\bar{u}_1$  is symmetric about the centerline and  $\bar{u}_3$  is antisymmetric about the centerline.

The transformation of the Reynolds stress tensor can also be obtained by employing Eq. (4) in the transformation (11c). The consequences for the stresses are such that all normal stresses and  $\overline{u_2u_3}$  are symmetric about the centerline. In contrast  $\overline{u_1u_2}$  and  $\overline{u_1u_3}$  are antisymmetric about the centerline. It should be noted that the results for  $\overline{u_1u_2}$  and  $\overline{u_2u_3}$  can also be obtained from the mean momentum Eqs. (1a) and (1c). The reflection properties of other one-point quantities such as the pressure-strain correlation and the dissipation tensor can also be determined by (12).

### 2.3 Lie group analysis of the two-point correlation equation

For simplicity it will be assumed in the following analysis that the Reynolds number tends to infinity so that the viscous terms in the two-point correlation equation (2) may be neglected. The basis for this assumption is the fact that, to leading order only, the large scales determine the mean velocity. Viscosity only affects the small scales of the order  $\mathcal{O}(\eta)$  where  $\eta$  is the Kolmogorov length scale. Hence neglecting viscosity is only valid for  $|\mathbf{r}| > \eta$ . If  $|\mathbf{r}| < \eta$ , the last term of the third line in Eq. (2) corresponds to the dissipation and cannot be neglected.

The general purpose of Lie group analysis, also called symmetry analysis, is two-fold. First, the symmetry transformations are to be determined, which give profound knowledge of the flow physics. Second, the symmetries may be used to achieve self-similarity or reduction of the two-point correlation equation. The first step to accomplish this objective is to find symmetry transformations which do not change the form of the equation under investigation. In fact, this is analogous to the analysis presented in the previous subsection where reflection symmetries have been investigated which do not alter the equations. However, the main difference in the present subsection is that the transformations considered therein are *finite* groups.

In order to obtain a reduction, *continuous* groups of transformations need to be considered. The method to find the desired continuous groups of transformations is called Lie group analysis. A good introduction to this method is given in Bluman and Kumei (1989) and Stephani (1989). In the present subsection only a heuristic approach will be presented while some more mathematical details on group methods are presented in Appendix B in Oberlack (1997a).

Self-similarity or reduction is always associated with the decrease of the number of independent variables. It is important to note that the independent variables are not necessarily restricted to the usual variables such as space and time. Instead any parameter in the equation under investigation may be considered as independent variable as long as it does not implicitly depend on any other independent parameter in the problem.

Hence, in the first step a reduction will be achieved by rewriting the two-point correlation equation as such that  $\Omega_1 \equiv \Omega$  is absorbed into all the remaining independent and dependent variables. The most general form of transformation allowing this reduction is

$$x_i = \tilde{x}_i \gamma(\Omega) \ , \quad r_i = \tilde{r}_i \gamma(\Omega) \ , \quad \bar{u}_i = \tilde{u}_i \gamma(\Omega) \Omega \ , \quad (13a)$$

$$R_{ij} = \tilde{R}_{ij} \gamma(\Omega)^2 \Omega^2 \ , \quad \overline{pu_i} = \widetilde{\overline{pu_i}} \gamma(\Omega)^3 \Omega^3 \ , \quad \overline{u_i p} = \widetilde{\overline{u_i p}} \gamma(\Omega)^3 \Omega^3 \ , \quad (13b)$$

$$R_{(ik)j} = \tilde{R}_{(ik)j} \gamma(\Omega)^3 \Omega^3 \ , \quad R_{i(jk)} = \tilde{R}_{i(jk)} \gamma(\Omega)^3 \Omega^3 \ , \quad (13c)$$

where the new variables are denoted by tilde, and  $\gamma(\Omega)$  is an arbitrary function of  $\Omega$ . After employing (13a-c) and imposing the high Reynolds number limit, the two-point correlation equations read

$$\begin{aligned} 0 = & -\tilde{R}_{2j} \delta_{i1} \frac{d\tilde{u}_1(\tilde{x}_2)}{d\tilde{x}_2} - \tilde{R}_{2j} \delta_{i3} \frac{d\tilde{u}_3(\tilde{x}_2)}{d\tilde{x}_2} - \tilde{R}_{i2} \delta_{j1} \frac{d\tilde{u}_1(\tilde{x}_2 + r_2)}{d(\tilde{x}_2 + \tilde{r}_2)} - \tilde{R}_{i2} \delta_{j3} \frac{d\tilde{u}_3(\tilde{x}_2 + r_2)}{d(\tilde{x}_2 + \tilde{r}_2)} \\ & - [\tilde{u}_1(\tilde{x}_2 + \tilde{r}_2) - \tilde{u}_1(\tilde{x}_2)] \frac{\partial \tilde{R}_{ij}}{\partial \tilde{r}_1} - [\tilde{u}_3(\tilde{x}_2 + \tilde{r}_2) - \tilde{u}_3(\tilde{x}_2)] \frac{\partial \tilde{R}_{ij}}{\partial \tilde{r}_3} \\ & - \frac{1}{\rho} \left[ \delta_{i2} \frac{\partial \widetilde{\overline{pu_j}}}{\partial \tilde{x}_2} - \frac{\partial \widetilde{\overline{pu_j}}}{\partial \tilde{r}_i} + \frac{\partial \widetilde{\overline{u_i p}}}{\partial \tilde{r}_j} \right] \\ & - \frac{\partial \tilde{R}_{(i2)j}}{\partial \tilde{x}_2} + \frac{\partial}{\partial \tilde{r}_k} \left[ \tilde{R}_{(ik)j} - \tilde{R}_{i(jk)} \right] - 2 \left[ e_{1li} \tilde{R}_{lj} + e_{1lj} \tilde{R}_{il} \right] \ . \end{aligned} \quad (14)$$

Obviously the set of independent variables  $x_2$ ,  $r_i$ , and  $\Omega$  has been reduced by one. From group theory it follows (see Appendix B in Oberlack 1997a) that the latter equation admits a further similarity reduction only for certain mean velocities which obey the equations

$$\begin{aligned} & [a_1(\tilde{x}_2 + \tilde{r}_2) + a_3 + a_5] \frac{d\tilde{u}_1(\tilde{x}_2 + \tilde{r}_2)}{d(\tilde{x}_2 + \tilde{r}_2)} - a_1 \tilde{u}_1(\tilde{x}_2 + \tilde{r}_2) \\ = & [a_1 \tilde{x}_2 + a_5] \frac{d\tilde{u}_1(\tilde{x}_2)}{d\tilde{x}_2} - a_1 \tilde{u}_1(\tilde{x}_2) \ , \end{aligned} \quad (15a)$$

$$\begin{aligned}
& [a_1(\tilde{x}_2 + \tilde{r}_2) + a_3 + a_5] \frac{d\tilde{u}_3(\tilde{x}_2 + \tilde{r}_2)}{d(\tilde{x}_2 + \tilde{r}_2)} - a_1 \tilde{u}_3(\tilde{x}_2 + \tilde{r}_2) \\
& = [a_1 \tilde{x}_2 + a_5] \frac{d\tilde{u}_3(\tilde{x}_2)}{d\tilde{x}_2} - a_1 \tilde{u}_3(\tilde{x}_2) , \tag{15b}
\end{aligned}$$

The corresponding similarity variables are to be obtained from the invariant surface condition (see e.g. Bluman & Kumei 1989)

$$\begin{aligned}
& \frac{d\tilde{r}_1}{a_1 \tilde{r}_1 + a_2} = \frac{d\tilde{r}_2}{a_1 \tilde{r}_2 + a_3} = \frac{d\tilde{r}_3}{a_1 \tilde{r}_3 + a_4} = \frac{d\tilde{x}_2}{a_1 \tilde{x}_2 + a_5} \\
& = \frac{d\tilde{R}_{ij}}{2a_1 \tilde{R}_{ij}} = \frac{d\widetilde{p\tilde{u}_i}}{3a_1 \widetilde{p\tilde{u}_i}} = \frac{d\widetilde{u_j\tilde{p}}}{3a_1 \widetilde{u_j\tilde{p}}} = \frac{d\tilde{R}_{(ik)j}}{3a_1 \tilde{R}_{(ik)j}} = \frac{d\tilde{R}_{i(jk)}}{3a_1 \tilde{R}_{i(jk)}} \tag{16}
\end{aligned}$$

where the constants of integration are taken as the new variables. The equations for the mean velocities above (15a,b) can only have a unique solution if

$$a_3 = 0. \tag{17}$$

Since each Eq. (15a-b) on the left-hand side depends on  $x_2 + r_2$  and on the right-hand side on  $x_2$ , they can only be equal if they are both equal to a constant. Hence, (15a,b) uniquely transfer to

$$[a_1 \tilde{x}_2 + a_5] \frac{d\tilde{u}_1(\tilde{x}_2)}{d\tilde{x}_2} - a_1 \tilde{u}_1(\tilde{x}_2) = c_1 , \tag{18a}$$

$$[a_1 \tilde{x}_2 + a_5] \frac{d\tilde{u}_3(\tilde{x}_2)}{d\tilde{x}_2} - a_1 \tilde{u}_3(\tilde{x}_2) = c_3 , \tag{18b}$$

Each of the parameters  $a_1$ - $a_5$  have a distinct physical meaning. The parameter  $a_1$  corresponds to the scaling group; i.e. Eq. (14) admits a transformation of the form

$$\tilde{x}_2^* = e^{a_1} \tilde{x}_2 , \quad \tilde{r}_i^* = e^{a_1} \tilde{r}_i , \quad \tilde{u}_i^* = e^{a_1} \tilde{u}_i , \tag{19a}$$

$$\tilde{R}_{ij}^* = e^{2a_1} \tilde{R}_{ij} , \quad \widetilde{p\tilde{u}_i}^* = e^{3a_1} \widetilde{p\tilde{u}_i} , \quad \widetilde{u_i\tilde{p}}^* = e^{3a_1} \widetilde{u_i\tilde{p}} , \tag{19b}$$

$$\tilde{R}_{(ik)j}^* = e^{3a_1} \tilde{R}_{(ik)j} , \quad \tilde{R}_{i(jk)}^* = e^{3a_1} \tilde{R}_{i(jk)} , \tag{19c}$$

which does not alter the functional form of the equation written in the new coordinates. The parameters  $a_2$ - $a_5$  correspond to the translation groups which conform to the fact that (14) is autonomous with respect to  $\tilde{x}_2$  and  $\tilde{r}_i$ . As a result (14) is invariant under transformations such as

$$\tilde{x}_2^* = \tilde{x}_2 + a_5 . \tag{20}$$

However, for physical reasons the translation invariance of  $\tilde{r}_i$  is not meaningful, and  $a_2$ - $a_4$  must be zero. In order to understand the problem with these ‘‘artificial’’ invariances, one has to call to mind that the translation invariance with respect to  $\tilde{r}_i$  gives rise to a new solution where the correlation function is shifted in correlation space. Since  $R_{ij}$  reaches its finite maximum at  $|\tilde{\mathbf{r}}| = 0$  and tends to zero for  $|\tilde{\mathbf{r}}| \rightarrow \pm\infty$ , a shift in the correlation space cannot be a new solution.

Depending on the value of  $a_1$ , two fundamentally different cases are to be distinguished for which a similarity reduction may be obtained.

2.2.1  $a_1 \neq 0$ 

The present case corresponds to the fact that scaling with respect to space is not inhibited and (18a,b) integrate to

$$\tilde{u}_1 = C_1 \left( \tilde{x}_2 + \frac{a_5}{a_1} \right) - \frac{c_1}{a_1} , \quad (21a)$$

$$\tilde{u}_3 = C_3 \left( \tilde{x}_2 + \frac{a_5}{a_1} \right) - \frac{c_3}{a_1} , \quad (21b)$$

where  $C_1$  and  $C_3$  are integration constants. If the transformation (13a) to the original coordinates is inferred, the latter equations read

$$\bar{u}_1 = C_1 \Omega x_2 + \Omega \gamma(\Omega) \left( C_1 \frac{a_5}{a_1} - \frac{c_1}{a_1} \right) , \quad (22a)$$

$$\bar{u}_3 = C_3 \Omega x_2 + \Omega \gamma(\Omega) \left( C_3 \frac{a_5}{a_1} - \frac{c_3}{a_1} \right) . \quad (22b)$$

It appears that the additive constants may depend on the rotation rate in an unknown manner. In order to resolve this problem, it is helpful to investigate the two-point correlation function.

Though a solid theoretical basis on first principles is still lacking, it appears that to leading order the two-point correlation function does not scale with the rotation rate  $\Omega$ . Hence it can be concluded from Eq. (13b) that, in order to have no  $\Omega$  dependence of  $R_{ij}$ , the function  $\gamma$  behaves as  $\gamma \sim 1/\Omega$ . As a result, the two additive constants appearing in the scaling laws (22a,b) do not depend on  $\Omega$  either. Only the slope of the linear scaling laws depends on the rotation rate.

The similarity variables for the case  $a_1 \neq 0$  corresponding to the mean velocities (21a,b) are to be obtained from the characteristic Eqs. (16). Employing  $a_2 = a_3 = a_4 = 0$ , the integration yields

$$\eta_1 = \frac{\tilde{r}_1}{\tilde{x}_2 + \frac{a_5}{a_1}} , \quad \eta_2 = \frac{\tilde{r}_2}{\tilde{x}_2 + \frac{a_5}{a_1}} , \quad \eta_3 = \frac{\tilde{r}_3}{\tilde{x}_2 + \frac{a_5}{a_1}} , \quad (23a)$$

$$\tilde{R}_{ij} = F_{ij} \left( \tilde{x}_2 + \frac{a_5}{a_1} \right)^2 , \quad \widetilde{\overline{p u_i}} = G_i \left( \tilde{x}_2 + \frac{a_5}{a_1} \right)^3 , \quad \widetilde{\overline{u_j p}} = H_j \left( \tilde{x}_2 + \frac{a_5}{a_1} \right)^3 , \quad (23b)$$

$$\tilde{R}_{(ik)j} = F_{(ik)j} \left( \tilde{x}_2 + \frac{a_5}{a_1} \right)^3 , \quad \tilde{R}_{i(jk)} = F_{i(jk)} \left( \tilde{x}_2 + \frac{a_5}{a_1} \right)^3 , \quad (23c)$$

where the integration constants  $\eta_i$ ,  $F_{ij}$ ,  $G_i$ ,  $H_i$ ,  $F_{(ik)j}$ , and  $F_{i(jk)}$  are the new similarity variables. In order to verify the similarity reduction of Eq. (14), the quantities  $F_{ij}$ ,  $G_i$ ,  $H_i$ ,  $F_{(ik)j}$ , and  $F_{i(jk)}$  are introduced as new dependent variables only depending on  $\eta_i$ .

In order to obtain a new identity in similarity space, the latter scaling is substituted into Eq. (6) for  $R_{ij}$ . For this purpose the origin of  $\tilde{x}_2$  may be chosen as such

$$\tilde{x}'_2 = \tilde{x}_2 + \frac{a_5}{a_1} \quad (24)$$

that the similarity variable simplifies to

$$\eta_i = \frac{\tilde{r}_i}{\tilde{x}'_2} \quad (25)$$

Introducing the transformation (23) into Eq. (6), we obtain the relation  $F_{ij}(\tilde{x}'_2, \tilde{x}'_2 \boldsymbol{\eta}) \cdot (\tilde{x}'_2)^2 = F_{ji}(\tilde{x}'_2(1 + \eta_2), -\tilde{x}'_2 \boldsymbol{\eta}) (\tilde{x}'_2)^2$ . Since it was previously assumed that all two-point correlation functions are solely functions of  $\boldsymbol{\eta}$ , only the ratio of the first and the second parameter can appear in  $F_{ij}$ . Thus, we finally obtain

$$F_{ij}(\boldsymbol{\eta}) = F_{ji} \left( \frac{-\eta}{1 + \eta_2} \right) . \quad (26)$$

The latter relation gives valuable insight into the structure of the solution. Relation (26) connects different  $\tilde{\mathbf{r}}$  domains to each other.

Interestingly enough, relation (26) gives raise to a new symmetry transformation

$$\tilde{\eta}_i = \frac{-\eta_i}{1 + \eta_2} \quad (27)$$

which is neither a reflection symmetry in the classical sense nor a continuous transformation (Lie group) since it does not contain a continuous parameter. Its validity can be verified by substituting (27) into Eq. (14) after the similarity coordinate (25) and the linear profiles (21a,b) have been employed.

One interesting feature of (26) is that it can be considered as an algebraic functional equation for the trace element of  $F_{ij}$  or  $R_{ij}$  in the following denoted as  $F_{[ii]}$  with  $i = 1, 2, 3$ . The ‘‘equilibrium’’ plane for Eq. (26) is  $\eta_2 = -2$  with arbitrary  $\eta_1$  and  $\eta_3$  where both the argument as well as the value of  $F_{ij}$  are the same. In addition  $\boldsymbol{\eta} = 0$  is an ‘‘equilibrium’’ point. Apart from these two regions, Eq. (26) defines a mapping between different  $\boldsymbol{\eta}$ -domains. There are two pairs of  $\eta_2$ -regions which map into each other, namely

$$\eta_2 : (-\infty, -2) \leftrightarrow (-2, -1) \quad \text{and} \quad (-1, 0) \leftrightarrow (0, \infty) . \quad (28)$$

The latter nomenclature refers to the fact that, once the functional values for  $F_{[ii]}$  in the  $\eta_2$  region  $(-2, -1)$  are known, the corresponding values in the region  $(-\infty, -2)$  are uniquely determined and vice versa. After a value for  $\eta_2$  is chosen, the values for  $\eta_1$  and  $\eta_3$  map according to

$$\frac{-\eta_1}{1 + \eta_2} \rightarrow \eta_1 \quad \text{and} \quad \frac{-\eta_3}{1 + \eta_2} \rightarrow \eta_3 \quad (29)$$

A graphical mapping scheme is given in Fig. 2. For clarity only the  $\eta_1$ - $\eta_2$  domain is depicted where connected mapping-regions are indicated by arrows. The extension to the entire  $\boldsymbol{\eta}$ -domain is straightforward.

Besides the above symmetry relation for  $F_{[ii]}$  with  $i = 1, 2, 3$ , (26) provides solutions for any off-diagonal  $F_{ij}$  element with ( $i \neq j$ ) if  $F_{ji}$  is known. Of course, similar features can be given for the pressure-velocity correlation and for the triple-correlation.

For the present case  $a_1 \neq 0$ , the statistical variables scale with the wall distance. This is different in the following subsection.

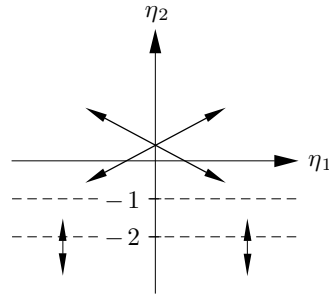


FIGURE 2. Non-locally related correlations in the  $\eta_1$ - $\eta_2$  plane according to Eq. (26).

### 2.2.2 $a_1 = 0$

The present subsection corresponds to the fact that scaling with respect to space is broken as can also be read from Eq. (19). As a result Eqs. (18a) and (18b) may be integrated to

$$\tilde{u}_1 = \frac{c_1}{a_5} \tilde{x}_2 + C_3, \quad (27a)$$

$$\tilde{u}_3 = \frac{c_3}{a_5} \tilde{x}_2 + C_4, \quad (27b)$$

where  $C_3$  and  $C_4$  are integration constants. The characteristic Eqs. (16) can not be integrated in the usual way. However, a reduction may still be possible since the correlation equation is autonomous in  $x_2$ . Due to the linear profile all statistical functions in (14) may not depend on the spatial coordinate  $\tilde{x}_2$ . Obviously, the present case corresponds to a homogeneous shear flow. Even though this does not appear to be a reduction in the usual sense from a group theoretical point of view, this is similar to the case  $a_1 \neq 0$ . In Section 2.2.1 a reduction was conducted by the scaling group ( $a_1$ ) while in the present case the reduction may be conducted by the translation group ( $a_5$ ). In both cases the dimensionality of the problem is reduced.

It should be noted that for physical reasons the case  $a_1 \neq 0$  appears to be more likely to be applicable to the rotating channel flow for the following reason. One of the key observations in Oberlack (1997a) was that turbulence has a tendency to establish a maximum degree of symmetry transformations. For the different channel flow cases, the highest degree of symmetry has been observed where the least wall influence is present, namely in the core region of the channel. Hence it may be expected that the same maximum principle applies for the present flow.

It is very important to note that the present analyses and, in particular, the one in Subsections 2.2.2 and 2.2.3 are not limited to the two-point correlation equation. The results regarding all the symmetries and scaling laws hold for all multi-point correlation equations up to any arbitrary order. Hence the closure problem of turbulence which usually precludes exact results do not form an obstacle for the present analysis.

More mathematical details on group methods and how to obtain the latter results can be found in appendix B of Oberlack (1997a).

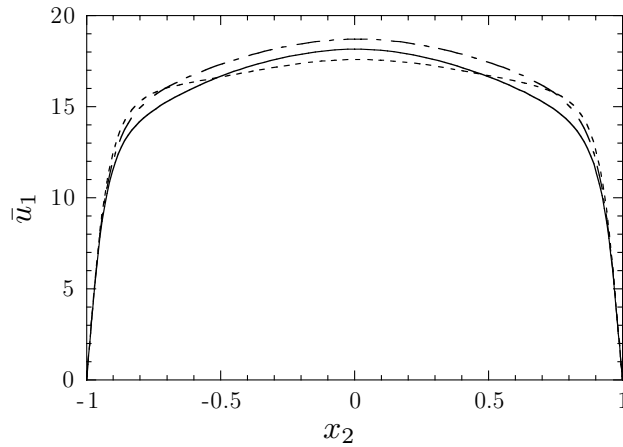


FIGURE 3. Streamwise mean velocity at  $Ro = 0$  —,  $Ro = 3.2$  ---- and  $Ro = 10$  - - - .

To conclude from the analysis, it is to be expected that a cone-shaped mean velocity in the streamwise direction will appear as such that the two flanks of the cone are linear. Furthermore, linear profiles for the cross flow will also establish on both sides of the centerline.

### 3. Direct numerical simulation of the flow

A DNS of the rotating channel flow has been conducted. The utilized numerical technique is a standard spectral method with a Fourier decomposition in streamwise and spanwise direction and a Chebyshev decomposition in wall-normal direction. The flow quantities are non-dimensionalized by  $h/2$  and  $u_\tau$  where  $h$  is the channel width and  $u_\tau$  is the friction velocity of the non-rotating case, which is defined as

$$\tau = u_\tau^2 = \left| \frac{1}{\rho} \frac{\partial \bar{p}}{\partial x_1} \right| \frac{h}{2} .$$

The density  $\rho$  is set to unity. The definition of the Reynolds number and its numerical value for all subsequent calculations below are

$$Re_\tau = \frac{hu_\tau}{2\nu} = 180 .$$

The rotation number is defined as

$$Ro = \frac{\Omega h}{u_\tau} .$$

The boundary conditions are non-slip at  $x_2 = \pm 1$  and periodic in  $x_1$ - and  $x_3$ -direction. The pressure-gradient is held constant for all computations. Further details on the numerical scheme may be obtained in Kim, Moin & Moser (1987).

Two computations at rotation numbers of  $Ro = 3.2$  and  $Ro = 10$  have been conducted. All presented results for  $Ro = 0$  have been taken from Kim, Moin &

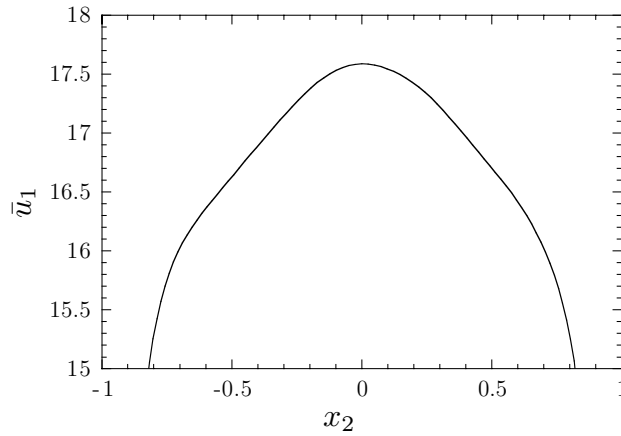


FIGURE 4. Streamwise mean velocity at  $Ro = 10$  in the core region.

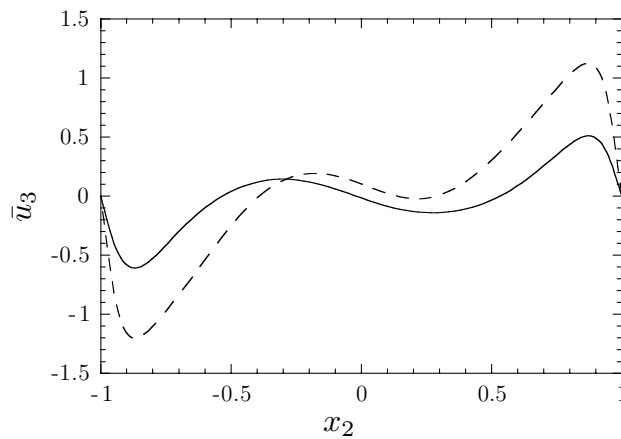


FIGURE 5. Spanwise mean velocity at  $Ro = 3.2$  — and  $Ro = 10$  ---- .

Moser (1987). The domain sizes used in the  $x_1$ ,  $x_2$ , and  $x_3$  directions are  $4\pi$ , 2, and  $4\pi/3$  on  $128 \times 129 \times 128$  grids, respectively, for the  $Ro = 0$  and 3.2 cases, and  $8\pi$ , 2, and  $2\pi$  on a  $256 \times 129 \times 128$  grid for the  $Ro = 10$  case. In Fig. 3 the streamwise mean velocity profiles at  $Ro = 0$ ,  $Ro = 3.2$ , and  $Ro = 10$  are compared. As expected from the global time scale analysis, the near-wall region up to  $x_2 = \pm 0.9$  is only marginally perturbed. Approaching the core region of the flow, a significant change in the mean velocity profile is visible with a very pronounced shoulder at  $x_2 = \pm 0.8$  for  $Ro = 10$ . In addition, a much flatter center region is noticeable. For the lower rotation rate no linear region is noticeable. It is interesting to note that an increase of mass flow is induced by the low rotation, which seems to disappear by increasing the rotation rate.

As predicted by the group analysis, two linear regions emerge on each side of the centerline for the high rotation rate. A more detailed perspective of the linear region is given in Fig. 4 where only the “head” of the profile for  $Ro = 10$  is depicted. The linear regions cover the wide range  $x_2 = 0.2 - 0.6$  on both sides of the center

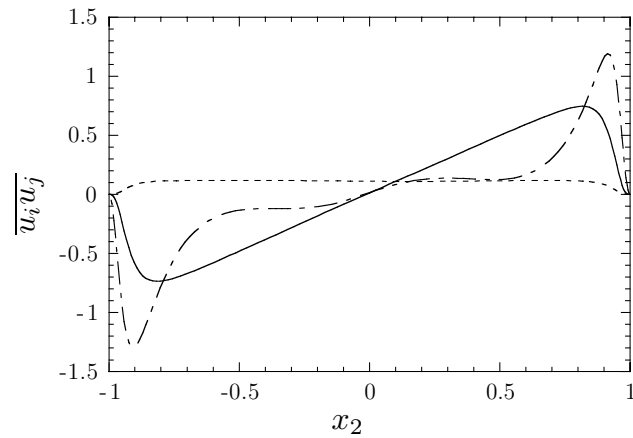


FIGURE 6. Shear stresses at  $Ro = 10$ :  $\overline{u_1 u_2}$  ———,  $\overline{u_2 u_3}$  - - - - ,  $\overline{u_1 u_3}$  - · - · .

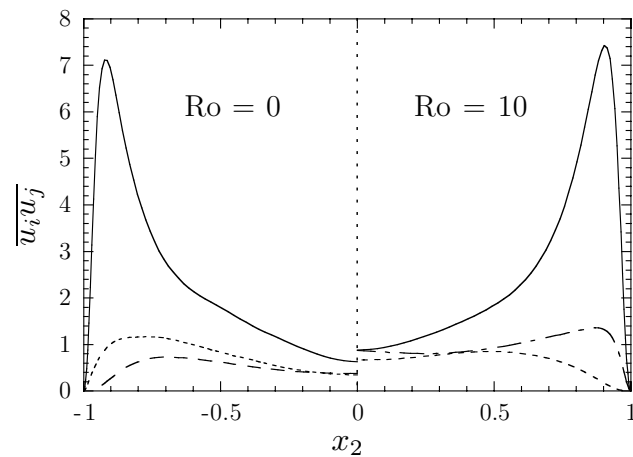


FIGURE 7. Normal stresses at  $Ro = 0$  on the left and  $Ro = 10$  on the right hand side:  $\overline{u_1 u_1}$  ———,  $\overline{u_2 u_2}$  - - - - ,  $\overline{u_3 u_3}$  - · - · .

line.

As already mentioned in Section 2, a mean cross flow denoted by  $\bar{u}_3$  is induced by the rotation. In Subsection 2.2 it was prognosticated that the flow is skew-symmetric about the centerline as shown in Fig. 5.

Though a still clearer verification is still lacking, it appears that the predicted linear profile is also visible in the induced crossflow. The location of the linear region is slightly shifted towards the wall region compared to the linear region of the streamwise velocity. One of the most interesting feature of the cross flow is the region near the centerline. Therein the cross flow has opposite sign compared to the flow regions closer to the channel walls. This large scale property of the flow may correspond to certain coherent structures; however, no such flow pattern could clearly be extracted from the flow so far.

From the statistical one-point quantities, only the Reynolds stress tensor has been computed. In Fig. 6 the Reynolds shear stresses at  $Ro = 10$  are displayed. Both the linear and the constant curves for  $\overline{u_1 u_2}$  and  $\overline{u_2 u_3}$  respectively can be derived from

the Eqs. (1a) and (1c) by neglecting the viscous terms, which are only significant in the near-wall region. One of the most intriguing features of the shear stresses is the induced  $\overline{u_1 u_3}$  component. The two other cross stresses can both be interpreted in terms of a simplified eddy-viscosity type of sense from its corresponding mean velocities. However, this cannot be done for the  $\overline{u_1 u_3}$  shear stress. Hence  $\overline{u_1 u_3}$  can only be modeled with the aid of more elaborate turbulence models such as LES or Reynolds stress transport models, to be presented in the next subsection.

In a corresponding DNS at  $Ro = 0$ , only the Reynolds shear stress  $\overline{u_1 u_2}$  is non-zero. The latter curve is not shown in Fig. 6 since both  $\overline{u_1 u_2}$  stress curves are very close to each other and only differ slightly in the near-wall region where viscosity is dominating the flow. All statistical curves exhibit the reflection symmetry properties about the centerline as has been found in Subsection 2.2.

The normal stresses for both the rotating and the non-rotating case are depicted in Fig. 7. Obviously, only very weak differences are noticeable compared to the strong change in the mean streamwise mean velocity induced by the rotation. Though the shape and magnitude of each set of curves for  $Ro = 0$  and  $Ro = 10$  are very similar, there are some distinct qualitative differences in the core region of the flow. We recall that the largest changes should be visible towards the core region of the flow as to be expected from the time scale analysis.

Many of the DNS results have to be considered as preliminary. For both the mean velocities and the stresses in Figs. 3-7, it is noticeable that the statistics is not fully converged. All cases presented previously bear the problem that the curves are not fully symmetric or skew-symmetric about the centerline. There are several problems leading to this deficiency.

A general problem with rotating flows is the fact that in order to get good statistics the required integration time of the computation is considerably longer than for the corresponding non-rotating case. This also appears to be an important issue for the present computation. Second, it is observed in the rotating pipe flow computation by Orlandi & Fatica (1998) and Eggels, Boersma & Nieuwstadt (1996) that very long coherent structures in the streamwise direction appear. This requires a very large computational box in order to ensure a sufficient decay to zero for the two-point correlation functions. In fact, for the present computation it was also noticed that the box in the spanwise direction needs to be larger than for the non-rotating channel flow. In Figs. 8-10 two-point correlations in both the streamwise and spanwise directions are shown. In Fig. 8 the two-point correlations in the streamwise direction for all normal stresses are shown at mid-plane ( $x_2 = 0$ ). Particularly, the spanwise component differs significantly from zero at  $x_1 = 5\pi$ . In Figs. 9 and 10 a wavy kind of two-point correlation is noticeable in the spanwise direction both at mid-plane ( $x_2 = 0$ ) as well as in the near-wall region at  $x_2 = -0.71$ . Except for the streamwise component at mid-plane, a substantial deviation from zero at  $x_3 = \pi$  is evident. From the latter findings it is apparent that a larger computation box both in the streamwise as well as in the spanwise direction is imperative to obtain more reliable, i.e. box independent results.

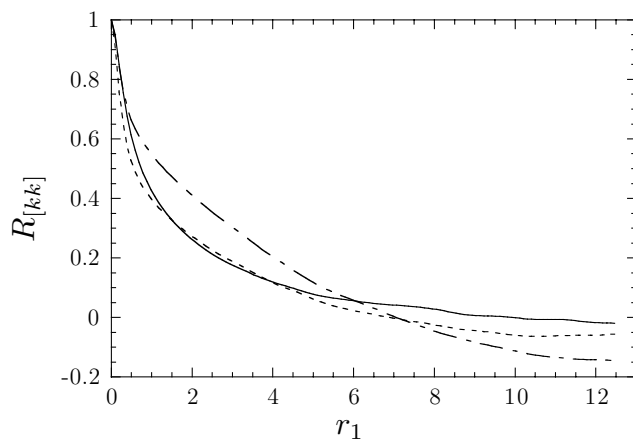


FIGURE 8. Two-point correlations in streamwise direction at mid-plane ( $x_2 = 0$ ) for  $Ro = 10$ :  $R_{11}$  ———,  $R_{22}$  - - - - ,  $R_{33}$  - · - · .

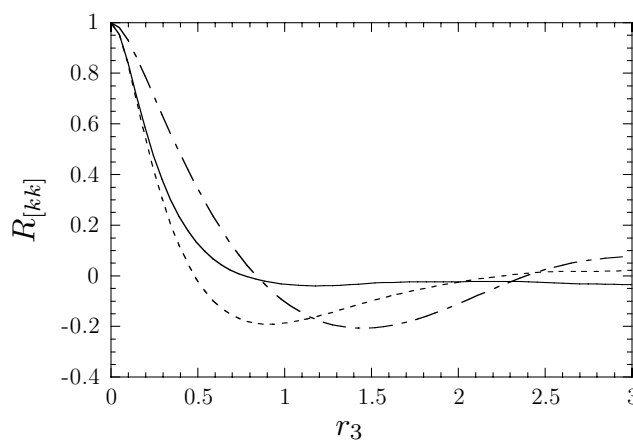


FIGURE 9. Two-point correlations in spanwise direction at mid-plane ( $x_2 = 0$ ) for  $Ro = 10$ :  $R_{11}$  ———,  $R_{22}$  - - - - ,  $R_{33}$  - · - · .

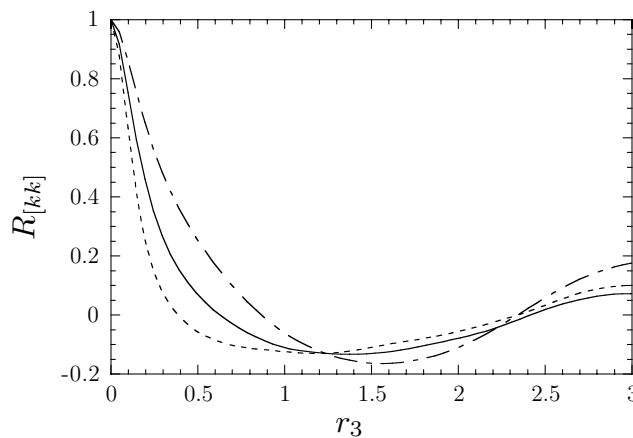


FIGURE 10. Two-point correlations in spanwise direction in the near-wall region ( $x_2 = -0.71$ ) for  $Ro = 10$ :  $R_{11}$  ———,  $R_{22}$  - - - - ,  $R_{33}$  - · - · .

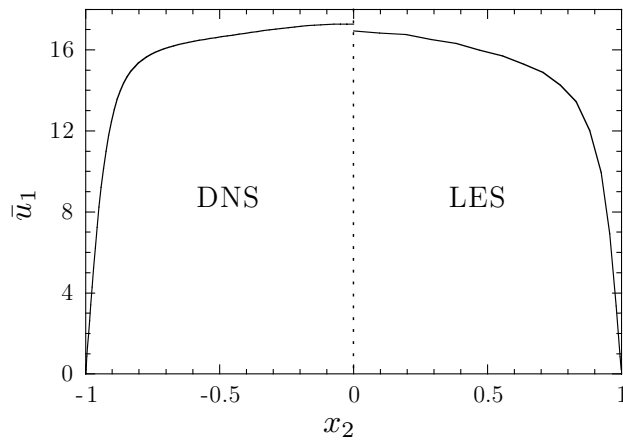


FIGURE 11. Streamwise mean velocity from DNS on the left- and LES on the right-hand side at  $Ro = 10$ .

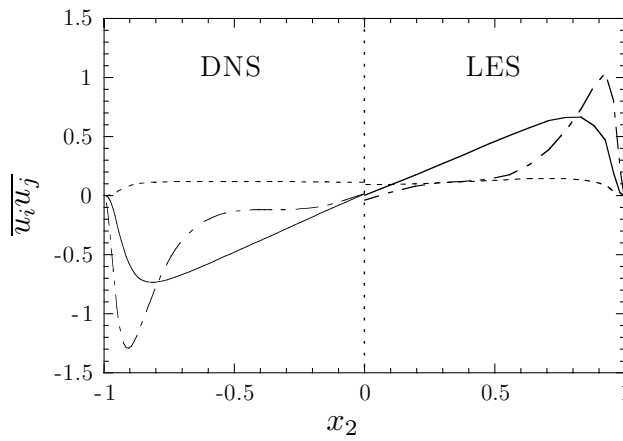


FIGURE 12. Shear stresses from the DNS on the left- and LES on the right-hand side at  $Ro = 10$ :  $\overline{u_1 u_2}$  ———,  $\overline{u_2 u_3}$  - - - - ,  $\overline{u_1 u_3}$  - · - · .

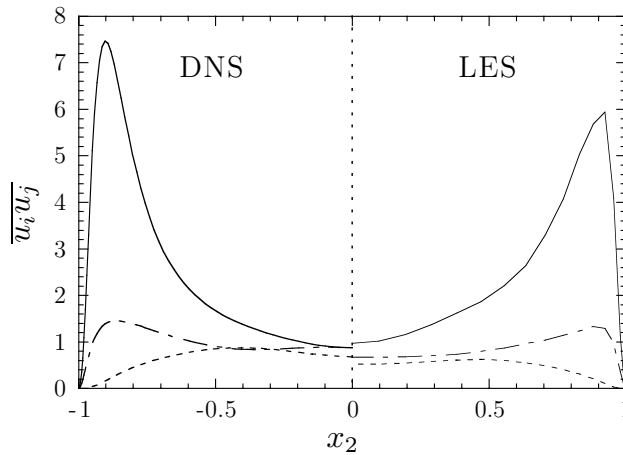


FIGURE 13. Normal stresses from the DNS on the left- and LES on the right-hand side at  $Ro = 10$ :  $\overline{u_1 u_1}$  ———,  $\overline{u_2 u_2}$  - - - - ,  $\overline{u_3 u_3}$  - · - · .

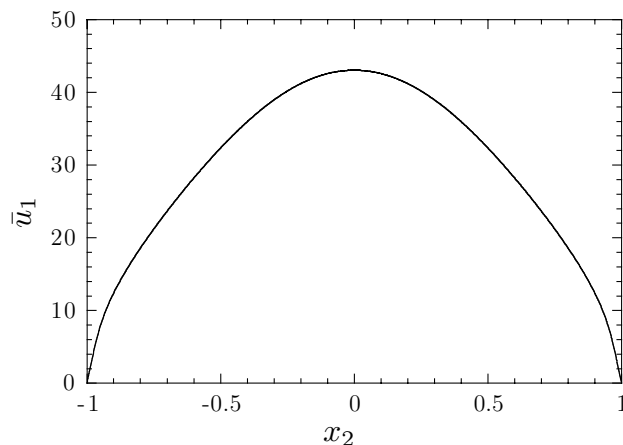


FIGURE 14. Streamwise velocity from the RANS model at  $Ro = 28$ .

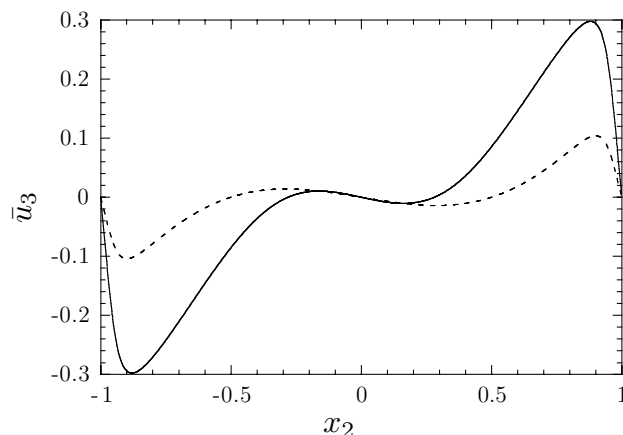


FIGURE 15. Spanwise velocity from the RANS model at  $Ro = 3.2$ : IP model —, SSG model ----.

#### 4. LES and second-moment closure models

System rotation is not a singular influence on the flow, but belongs to a wider class of benchmarks which mimics mean streamline curvature. This is very important for almost any application. Since system rotation is a challenging measure for turbulence models, we have investigated the response of two classes of turbulence models on the influence of streamwise rotation on the turbulent channel flow. First, LES of turbulence has been investigated. Thereafter, second-moment closure has been employed to test its ability to model the flow. Classical two-equation models such as the  $k-\varepsilon$  or the  $k-\omega$  model have not been examined since they exhibit no reaction on system rotation. This inability can directly read off from the model equations since no Coriolis type of term appears in the transport equation for the statistical quantities.

The first turbulence model to be investigated is the dynamic subgrid-scale model (Germano *et al.* 1991, Lilly 1992) used in LES. Since the dynamic model is “2D

material-frame indifferent" (see Speziale 1981 and Oberlack 1997b), one may expect that at least in the limit of large rotation numbers the model should capture the trends observed in the DNS. Interestingly enough, it will be seen subsequently that the dynamic model captures very well most of the trends in the flow even quantitatively except for the linear regions in the streamwise mean velocity. The flow parameters and the numerical scheme are the same as for the DNS. The grid sizes in  $x_1$ ,  $x_3$ , and  $x_4$  direction are 48, 32, and 32 respectively for the  $Ro = 0$  and 3.2 cases, and  $96 \times 33 \times 48$  for the  $Ro = 10$  case.

In Fig. 11 the streamwise mean velocities from DNS and LES are compared. Even though the LES profile changes significantly due to the system rotation it does not exhibit a clear linear region as was observed in the DNS. In addition, the mass flux is marginally smaller than in the DNS.

In Fig. 12 the shear stresses from the DNS are very well represented by the LES calculation. Even quantitative results show close agreements with the DNS. The normal stresses in Fig. 13 exhibit less good agreement with the DNS, but a correct qualitative agreement is clearly visible. In particular, the near-wall peak of  $\overline{u_1 u_1}$  is too low compared to the DNS. A general trend is that all Reynolds stress profiles in the LES are somewhat lower than in the DNS. Apparently, the sub-grid scale model produces slightly too much damping, which is particularly noticeable in the  $\overline{u_1 u_1}$  and  $\overline{u_1 u_3}$  stress component.

The second turbulence model to be investigated for the present type of flow is a second-moment closure model. The equations are based on the IP model (see Launder, Reece & Rodi 1975) and the SSG model (see Speziale, Sarkar & Gatsi 1989) for the pressure-strain term. The near-wall behavior of the pressure-strain term is modeled by the elliptic-relaxation approach developed by Durbin (1991,1993). The equation for the dissipation of turbulent kinetic energy is taken from the Launder-Reece-Rodi model. Model parameters have been taken from the original publications and have not been altered for the present computation.

Some general remarks should be made before some results from the second-moment model will be presented. Investigating the structure of the model equations, it appears that the linear region of the mean velocities may lead to a reduction of variables and hence to self-similarity. This is essentially due to the fact that the model equations contain Coriolis type of terms. This is in clear contrast to classical two-equation models. Besides the usual Coriolis terms, the rotation rate only appears in the pressure-strain model and not in the dissipation equation. Since the cross flow and the stress components  $\overline{u_2 u_3}$  and  $\overline{u_1 u_3}$  are solely induced by the rotation, it is the pressure-strain model in particular which determines these quantities. As a result it will subsequently be seen that the cross flow is particularly sensitive to the pressure-strain model though the general flow pattern is captured with all models.

The turbulent diffusion terms have a very strong influence on the model results. Hence the linear regions in the streamwise velocity are only visible at very high rotation rates for which DNS results have not been obtained yet. In Fig. 14 the streamwise velocity is shown for the very high rotation number  $Ro = 28$  obtained

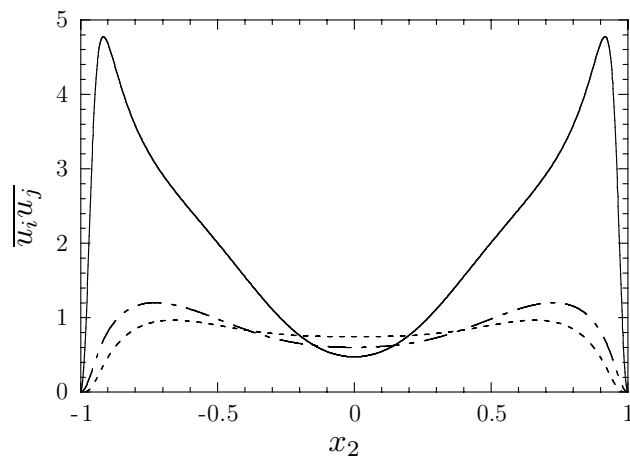


FIGURE 16. Normal stresses from the SSG model at  $Ro = 10$ :  $\overline{u_1 u_1}$  —,  $\overline{u_2 u_2}$  ----,  $\overline{u_3 u_3}$  -.-.

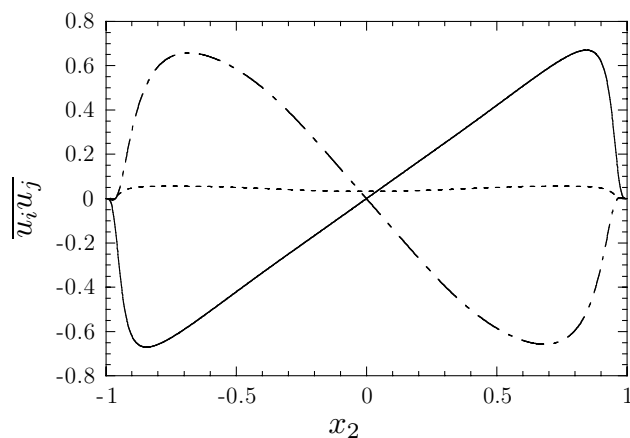


FIGURE 17. Shear stresses from the SSG model at  $Ro = 10$ :  $\overline{u_1 u_2}$  —,  $\overline{u_2 u_3}$  ----,  $\overline{u_1 u_3}$  -.-.

with the IP model. Almost identical results are obtained with the SSG model not presented here.

In contrast to this, the cross flow is extremely sensitive to the implemented pressure-strain model. In Fig. 15 the spanwise velocities for the IP and the SSG model are compared at  $Ro = 3.2$ . Apparently the shape of the DNS curve in Fig. 5 is represented by both models. However, both absolute values of the  $\bar{u}_3$  velocities are very much underpredicted. Even the maximum of the SSG model is underpredicted by a factor of two.

Much less sensitive to the pressure-strain model are the normal stresses. In Fig. 16 the normal stress from the SSG model are presented. It is interesting to note that not only the overall property of the DNS data are modeled quite well represented, but also that a quantitative agreement within 30% is obtained. This has been obtained without adjusting any model coefficients.

In contrast to this, it can be seen in Fig. 17 that from the shear stresses only

$\overline{u_1 u_2}$  is obtained with reasonable agreement compared to the DNS results. Of course, this is due to fact that  $\overline{u_1 u_2}$  is merely determined by the mean momentum equation, which does not contain any modeled terms. Though an almost constant  $\overline{u_2 u_3}$  component is obtained in the center region of the flow as predicted by the DNS, its value is much too small. Regarding the  $\overline{u_1 u_3}$  stress component, one has to conclude that the model equation is not even able to model the proper trends of the DNS results. The sign of  $\overline{u_1 u_3}$  disagrees with the result from the DNS.

## 5. Summary and conclusions

The general purpose of the present work is to establish a new but still very simple canonical test case to study basic turbulence physics. It has been confirmed by DNS that there are linear regions in both the streamwise and the spanwise mean velocity as was suggested by Lie group analysis of the two-point correlation equations. Additional scaling properties of the two-point correlation functions have been established.

Beside the mean flow, all Reynolds stress quantities have been computed. It is interesting to note that, in contrast to the classical rotating channel flow, all six Reynolds stress components are non-zero. The stress components from the DNS have the expected symmetry properties about the centerline as predicted by the symmetry analysis.

The flow is very challenging for turbulence models since common two-equation models can not account for the rotation effects. Both LES with the dynamic subgrid-scale model and second-moment models have been tested for the present flow geometry. The LES captures most of the DNS results very well. Only the linear regions in the streamwise velocity were not visible. Employing a second-moment model, some basic trends of the flow have been captured. However, several serious drawbacks have been encountered. This is, in particular, that the linear region in the streamwise velocity was only visible for very high rotation rates. In addition, the induced cross flow had the proper shape but was extremely sensitive to the employed pressure-strain model. Finally, most of the qualitative tendencies in the Reynolds stresses were captured except for the  $\overline{u_1 u_3}$  component, which showed the opposite sign to that obtained by the DNS.

Future extensions of the project may be manifold. First, a larger computational domain need to be utilized to obtain more reliable results for the two-point correlation functions. Second, a much longer time integration time is mandatory in order to obtain better turbulence statistics. In addition, a higher rotation rate may be investigated to verify certain trends such as the linear scaling. Also, other scaling and symmetry properties described in Section 2 may be verified by the numerical data. Finally, other turbulence properties such as statistical quantities or coherent structures can also be analyzed from the data.

## REFERENCES

- BLUMAN, G. W. & KUMEI, S. 1989 *Symmetries and Differential Equations*. Applied mathematical sciences, vol. 81, Springer.

- DURBIN, P. 1991 Near-wall turbulence closure modeling without ‘damping functions’. *Theoret. Comput. Fluid Dyn.* **3**, 1-13.
- DURBIN, P. 1993 A Reynolds stress model for near-wall turbulence. *J. Fluid Mech.* **249**, 465-498.
- EGGELS, J. G. M., BOERSMA, B. J. & NIEUWSTADT, F. T. M. 1996 Direct and large eddy simulation of turbulent flow in an axially rotating pipe. Submitted to *J. Fluid Mech.*
- GERMANO, M., PIOMELLI, U., MOIN, P., & CABOT, W. H. 1991 A dynamic subgrid-scale eddy viscosity model. *Phys. Fluids A*. **3**, 1760-1765. Erratum: *Phys. Fluids A* **3**, 3128.
- HINZE, J. O. 1959 *Turbulence*, McGraw-Hill, NY, reissued 1975 and 1987.
- JOHNSTON, J. P., HALLEEN, R. M. & LAZIUS, D. K. 1972 Effects of spanwise rotation on the structure of two-dimensional fully developed turbulent channel flow. *J. Fluid Mech.* **56**, 533-557.
- KIM, J., MOIN, P. & MOSER, R. 1987 Turbulence statistics in fully developed channel flow at low Reynolds number. *J. Fluid Mech.* **177**, 133-166.
- KRISTOFFERSEN, R. & ANDERSSON, H. I. 1993 Direct simulations of low-Reynolds-number turbulent flow in a rotating channel. *J. Fluid Mech.* **256**, 163-197.
- LILLY, D. 1992 A proposed modification of the Germano subgrid-scale closure method. *Phys. Fluids A*. **4**, 633-635.
- OBERLACK M. 1994 Derivation and Solution of a New Length Scale- and Dissipation-Tensor Equation for Turbulent Flows, *Doctor's Thesis RWTH Aachen, Germany*.
- OBERLACK M. 1995 Analysis of the Two-Point Velocity Correlations in Turbulent Boundary Layer Flows, *Annual Research Briefs*. Center for Turbulence Research, NASA Ames/Stanford Univ., 209-220.
- OBERLACK, M. 1997a Unified Theory for Symmetries in Plane Parallel Turbulent Shear Flows, *Manuscript no. 163*, Center for Turbulence Research, NASA Ames/Stanford Univ., under review in *J. Fluid Mech.*
- OBERLACK, M. 1997b Invariant modeling in large-eddy simulation of turbulence, *Annual Research Briefs*, Center for Turbulence Research, NASA Ames/Stanford Univ., 3-22.
- ORLANDI, P. & FATICA M. 1997 Direct simulations of turbulent flow in a pipe rotating about its axis. *J. Fluid Mech.* **343**, 43-72.
- ROTTA, J. C. 1972 *Turbulente Strömungen*, Teubner Stuttgart.
- SPEZIALE, C. G. 1981 Some Interesting Properties of Two-Dimensional Turbulence. *Phys. Fluids A*. **28**(8), 1425-1427.
- STEPHANI, H. 1989 *Differential Equations: Their Solution using Symmetries*. edited by Malcolm MacCallum, Cambridge University Press.